Supporting Information

Interface Engineering in Hierarchical Assembly of Carbon-confined Fe_3O_4 Nanospheres for Enhanced Microwave Absorption

*Xiaofeng Shi,[1, 3] Zhengchen Wu,[1] Zhengwang Liu,[1] Lv Jianguo,[3] Zi Zhenfa,[3] and Renchao Che[1, 2,] **

1 Laboratory of Advanced Materials, Shanghai Key Lab of Molecular Catalysis and Innovative Materials, Fudan University, Shanghai 200438, P. R. China

2 Department of Materials Science, Fudan University, Shanghai 200438, P. R. China

3 School of Physics and Materials Engineering, and Key Laboratory for Photoelectric Detection Science and Technology of Education Department of Anhui Province, Hefei Normal University, Hefei 230601, PR China

* E-mail: rcche@fudan.edu.cn

S1: Experimental section

Chemical material

Ferric chloride hexahydrate ($FeCl_3 \cdot 6H_2O$), polyethylene glycol (PEG), ethylene glycol (EG), ethanol, sodium acetate and dopamine hydrochloride were purchased from Shanghai Sinopharm Chemical reagent Co. Ltd. All agents were directly used without further purification. Ultrapure water from the Milli-Q system (Millipore, Bedford, MA) was used in the following experiments.

Material synthesis

Preparation of Fe_3O_4 microspheres

$FeCl_3 \cdot 6H_2O$ (5.4 g) and PEG (4.0 g) were dissolved into ethylene glycol (160 mL) to form a clear solution, followed by sodium acetate (4.8 g). Subsequently, the mixture was transferred into a Teflon-lined stainless-steel autoclave (200 mL) and heated at 200 °C for 3 d. The black products were collected by a magnet, washed with deionized water and absolute ethanol three times, and dried at 60 °C in a vacuum oven.

Preparation of hierarchical Fe_3O_4@C and core-shell Fe_3O_4@C microsphere

The as-prepared Fe_3O_4 microspheres (0.2 g) were ultrasonically dispersed in deionized water (200 ml). The tris(hydroxymethyl) aminomethane (0.2423 g) was then added into the solution, followed by the addition of dopamine hydrochloride (0.2 g). The mixed solution was

mechanically stirred for 30 min. The products were washed with water and ethanol dried at 60 °C in vacuum. Finally, the powder was calcined under an N_2 atmosphere in a tube furnace at 500 °C for 3 h. The as-obtained hierarchical Fe_3O_4@C microsphere was denoted as H-Fe_3O_4@C. As a contrast, the core-shell Fe_3O_4@C microsphere was prepared by the same polydopamine coating and calcination process. Differently, the Fe_3O_4 microspheres were synthesized via a solvothermal method previously reported[1].

Characterization

The TEM image, HRTEM, SAED, EDS were acquired on field-emission transmission electron microscope (TEM, JEOL, JEM-2100F) at an acceleration voltage of 200 kV. The morphology and size were analyzed by field-emission scanning electron microscope ((FESEM, HITACHI, S-4800) operated at 1.0 kV. X-ray diffraction (XRD) spectra was obtained using a X-ray diffractometer with Ni-filtered Cu Kα radiation (Bruker, 40 kV, 40mA) in the 2θ range of 10°~ 90° at the scanning rate of 10° min^{-1}.. Magnetic properties were characterized by superconducting quantum interference device (SQUID) and electron holography (JEM-2100F). The X-ray photoelectron spectroscopy (XPS) was performed using a KRATOS Axis Ultra DLD equipped with a monochromatic X-ray source. The complex relative permittivity and permeability were measured by an N5230C vector network analyzer, and the detailed procedure was

described in the Supporting Information.

S2: The details of conventional electromagnetic measurements

The as-obtained powder of hierarchical Fe chains is homogeneously mixed in the paraffin wax referring to a mass ratio of 3:1. Then the mixture is poured into hollow model with 7.00 mm outer diameter and 3.00 mm inner diameter. The complex relative permittivity and permeability were measured by an N5230C vector network analyzer in the 2-18 GHz range. The reflection loss (RL) values serve as a crucial standard to microwave absorption performance, which can be calculated via the transmit line theory, described as follows:

$$Z = |Z_{in}/Z_0| = \sqrt{|\mu_r/\varepsilon_r|}tanh\left[j\left(\frac{2\pi f d}{c}\right)\sqrt{\mu_r\varepsilon_r}\right] \quad (1)$$

$$RL = 20log\left|(Z_{in} - Z_0)/(Z_{in} + Z_0)\right| \quad (2)$$

Where *f* refers to the frequency, d is the thickness of the absorber, and c is the light velocity, respectively.

S3. The holography method

Off-axis electron holography is a powerful technique to determine the phase shift of electron wave caused by magnetic and electric fields in its traveling path. The fundamental principle of holography is expounded as follows. In the TEM system, both the reference electron wave and object wave deflected by electrostatic biprism. These two waves converge and form an interference wave on the observation plane. The CCD camera can record the intensity distribution of the interference wave, which is also

known as the hologram. Through a sequential process of FFT, inverse FFT, and filter method, the distribution of object wave phase can be reconstructed by the hologram. According to classical electromagnetism, the electron wave phase can be converted into magnetic induction intensity and electric potential. Therefore, the magnetic flux density distribution and electric charge distribution of objective area are measured. The phase reconstruction is carried out by software package Holoworks 5.0 in Gatan DigitalMicrogaph. On the basis of the simplified Poisson's equation of electrostatic field theory and related variation factors, the charge density of materials can be calculated by the follow equation:

$$\rho(\chi) = -\varepsilon_{\gamma}\varepsilon_{0}\frac{\partial^{2}v(\chi)}{\partial x\chi^{2}}$$

Where ρ(x) is the charge density, x is the distance, and ε_{γ} and ε_{0} are the relative dielectric constant in the sample and the dielectric constant in vacuum, respectively.

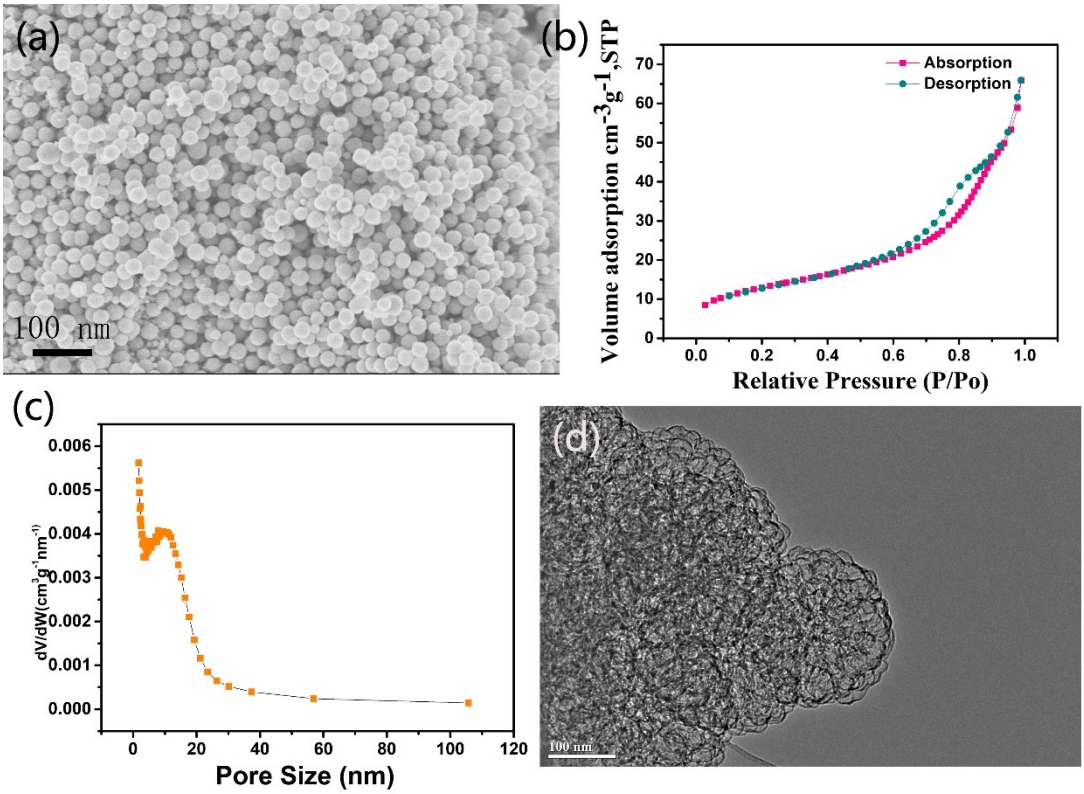

Figure S1. (a) SEM images of Fe_3O_4 microspheres, (b, c) N_2 adsorption–desorption isotherms and pore size distribution of Fe_3O_4 microspheres. (d) As-obtained carbon nanocages after etching Fe_3O_4 cores.

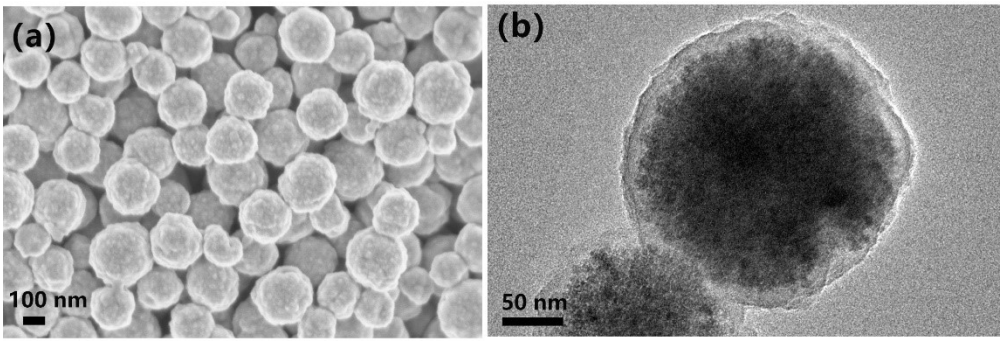

Figure S2. SEM and TEM images of the Core-shell Fe_3O_4@C microsphere.

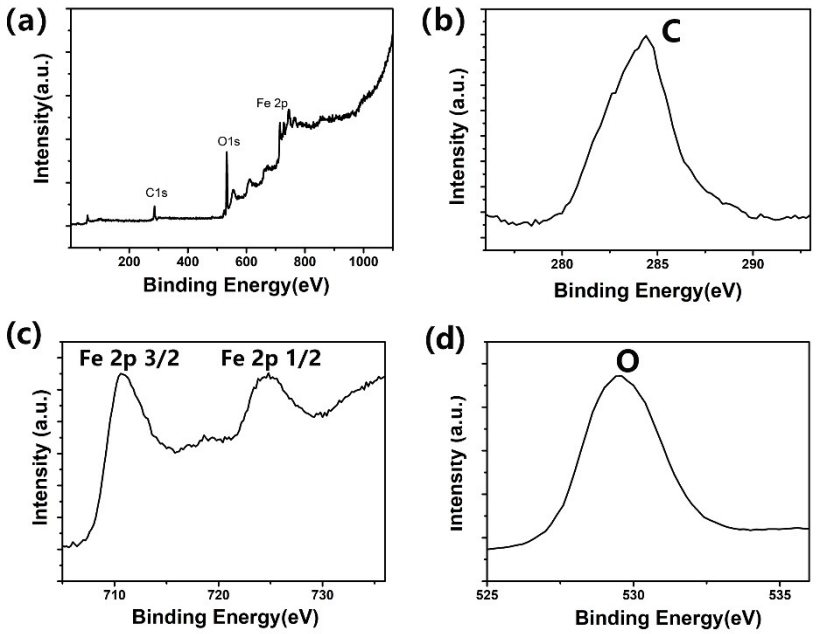

Figure S3. XPS spectra for hierarchical Fe_3O_4@C microsphere.

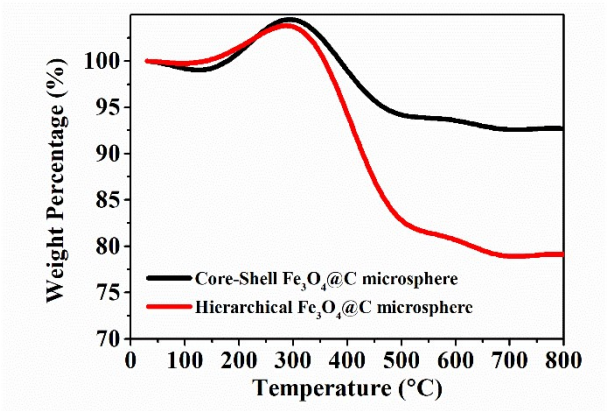

Figure S4. The TGA curves of core-shell Fe_3O_4@C microsphere and hierarchical Fe_3O_4@C microsphere.

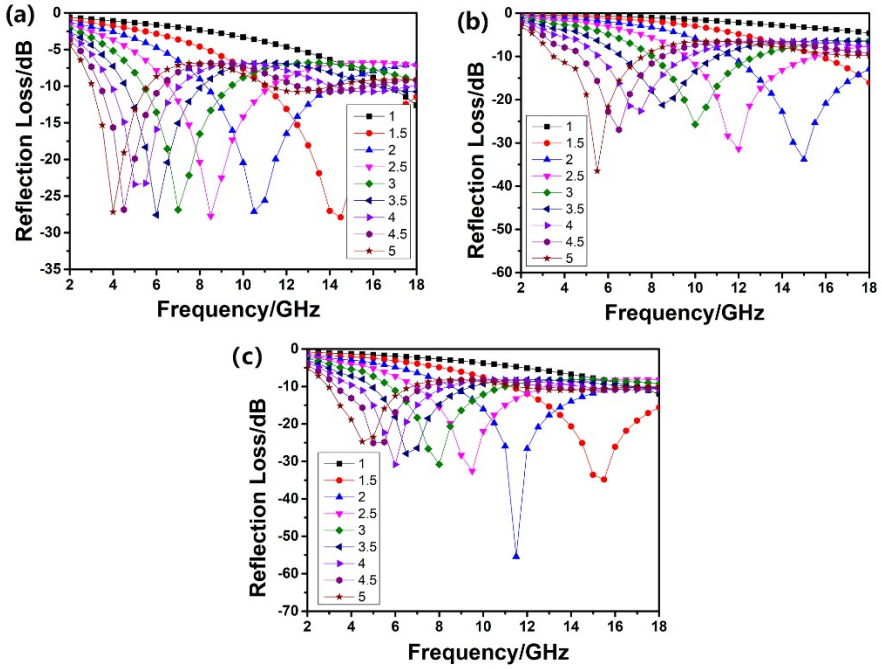

Figure S5. Frequency dependence of microwave RL curves of the samples: (a) Fe_3O_4 microsphere. (b) core-shell Fe_3O_4@C microsphere. (c) hierarchical Fe_3O_4@C microsphere.

Table S1. Comparison of microwave absorption performance between the prepared absorbers with carbon-based magnetic-dielectric components.

Absorbers	Optimal RL (dB)	Frequency range (GHz) (RL < –10dB)	References
CoNi@C nanosheets	-43.7	5.7	2
Fe_3O_4@C	-18.8	4.2	3
FeCo@carbon	-67.8	5.3	4
FeCo/C nanocages	-47.6	8.9	5
Carbon Spheres	-39.3	9.1	6
Bowl-like Co/C	-42.3	5.1	7
Fe_3O_4@C nanoring	–28.7	8.3	8
Magnetic carbon	-52.0	5	9
Ni@C microspheres	-73.2	4.8	10
NiCo@C/ZnO	-60.9	6.08	11
Fe-C nanofibers	-36.0	0.9	12
FeCo/CNTs	-46.5	3.92	13
Fe–Fe_3C@C	–28.1	4.1	14
Multishell Ag/C	–19.6	5.85	15
porous Ni/C	–28.4	4.5	16
NiCo/C	−58.8	6.8	17
H-Fe_3O_4@C	-55.4	9.5	herein

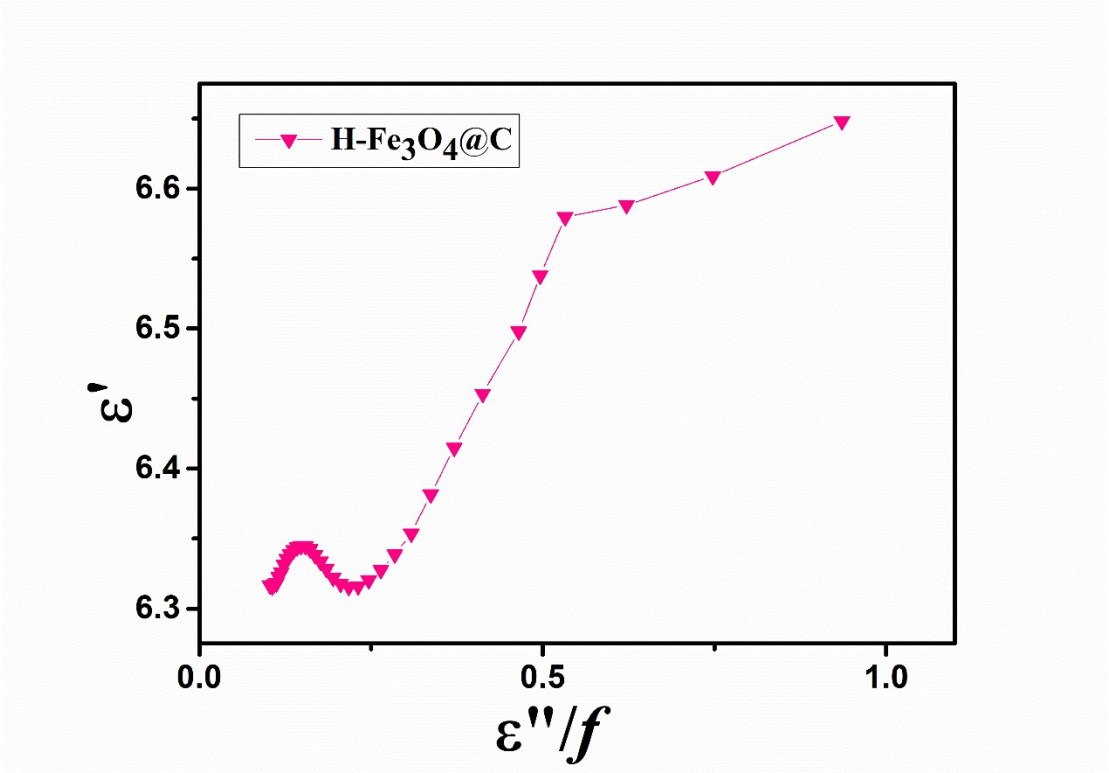

Figure S6. The plots of ε' versus ε''/*f* of the hierarchical Fe_3O_4@C microsphere.

References

1. X. F. Shi, Z. W. Liu, X. Li, W. B. You, Z. Z. Shao and R. C. Che, *Chem. Eng. J.*, 2021, **419**, 130020.
2. X. Liang, Z. Man, B. Quan, J. Zheng, W. Gu, Z. Zhang and G. Ji, *Nano-Micro lett.*, 2020, **12**, 1-12.
3. Y. Du, W. Liu, R. Qiang, Y. Wang, X. Han, J. Ma and P. Xu, *ACS Appl. Mater. Interfaces*, 2014, **6**, 12997-13006.
4. F. Wang, N. Wang, X. Han, D. Liu, Y. Wang, L. Cui, P. Xu and Y. Du, *Carbon*, 2019, **145**, 701-711.
5. Y. Xiong, L. Xu, C. Yang, Q. Sun and X. Xu, *J. Mater. Chem. A*, 2020, **8**, 18863-18871.

6. Y. Song, F. Yin, C. Zhang, W. Guo, L. Han and Y. Yuan, *Nano-Micro lett.*, 2021, **13**, 1-16.

7. J. Liang, J. Chen, H. Shen, K. Hu, B. Zhao and J. Kong, *Chem. Mater.*, 2021, **33**, 1789-1798.

8. N. Li, G.-W. Huang, Y.-Q. Li, H.-M. Xiao, Q.-P. Feng, N. Hu and S.-Y. Fu, *ACS Appl. Mater. Interfaces*, 2017, **9**, 2973-2983.

9. H. Zhao, Y. Cheng, H. Lv, G. Ji and Y. Du, *Carbon*, 2019, **142**, 245-253.

10. D. Liu, Y. Du, P. Xu, N. Liu, Y. Wang, H. Zhao, L. Cui and X. Han, *J. Mater. Chem. C*, 2019, **7**, 5037-5046.

11. J. Wang, Z. Jia, X. Liu, J. Dou, B. Xu, B. Wang and G. Wu, *Nano-Micro Lett.*, 2021, **13**, 1-16.

12. T. Wang, H. D. Wang, X. Chi, R. Li and J. B. Wang, *Carbon*, 2014, **74**, 312-318.

13. B. Yang, Y. Wu, X. P. Li and R. H. Yu, *Mater. Design*, 2017, **136**, 13-22.

14. X. Jian, X. Y. Xiao, L. J. Deng, W. Tian, X. Wang, N. Mahmood and S. X. Dou, *ACS Appl. Mater. Interfaces*, 2018, **10**, 9369-9378.

15. J. T. Zhou, J. Q. Tao, Z. J. Yao, L. L. Xu, Z. Li and P. Chen, *ACS Appl. Nano. Mater.*, 2021, **4**, 5425-5436.

16. S. Qiu, H. L. Lyu, J. R. Liu, Y. Z. Liu, N. N. Wu and W. Liu, *ACS Appl. Mater. Interfaces*, 2016, **8**, 20258-20266.

17. L. Wang, B. Wen, X. Y. Bai, C. Liu and H. B. Yang, *ACS Appl. Nano. Mater.*, 2019, **2**, 7827-7838.